Time-domain analysis of dispersive transmission lines

Wojciech Gwarek, Malgorzata Celuch-Marcysiak

Classification
Physics Abstracts
41.90 — 02.60

Time-domain analysis of dispersive transmission lines

Wojciech Gwarek ([1]) and Malgorzata Celuch-Marcysiak ([2])

([1]) LEST CNRS 1429 ; Dept. ELP, Ecole Nationale Supérieure de Télécommunications de Bretagne, B.P. 832, 29-285 Brest, France
([2]) Instytut Radioelektroniki, Politechnika Warszawska, 00-665 Warszawa, Nowowiejska 15/19, Poland

(*Received 17 March 1992, revised 3 November 1992, accepted 6 November 1992*)

Abstract. — We present and compare three time domain algorithms for calculating the dispersion characteristics of transmission lines of arbitrary cross-section : the 2-DV FD-TD, the Complex SCN TLM and the 2-DV SCN TLM proposed in this work. All the algorithms prove efficient, as a result of reducing the numerical analysis to two space dimensions. Their accuracy is demonstrated by means of comparison with the results obtained by other methods, for a range of practical examples of microwave guiding structures. We also introduce a new type of excitation which further improves the efficiency and reliability of the time-domain approach.

1. Introduction.

The problem of analyzing waves in transmission lines is of great importance in various frequency ranges. It becomes particularly pronounced in the microwave frequency region where the dispersion characteristics and field distribution of various modes have to be known for proper designing of a microwave circuit. Fundamentally, the problem of analyzing waves in guiding structure is three-dimensional. However, a direct three-dimensional approach is not attractive for a designer. For each value β of a propagation constant along the guide, the three-dimensional approach involves resonating a section of the guide of length $L = \pi/\beta$. This leads to extensive requirements of memory space and computing time.

A way to overcome this efficiency problem follows from the realization that for each assumed value of the propagation constant β an analytical description of fields along the guide is known. Thus the numerical analysis can be reduced to two-dimensional calculations of the guide's cross-section. This approach is basically the same as elimitating the time variable in circuit theory of sinusoidally excited circuits.

In the paper we consider three time-domain algorithms utilizing the above approach :

i) the specially adapted version of the finite-difference time-domain [2] which we will call 2-DV FD-TD ;

ii) the TLM algorithm based on the symmetrical condensed node with arms closed in a loop along the analyzed guide [3] which we will call Complex SCN TLM ;

iii) the improved TLM algorithm based on the specially transformed symmetrical condensed node introduced in this work which we will call 2-DV SCN TLM.

We present the accuracy and versatility of the time-domain algorithms for the full-wave analysis of arbitrary guiding structures. We discuss relative advantages and disadvantages of the three time-domain algorithms, considering in particular their effectiveness. We finally reveal the possibility to further improve the speed and reliability of the time-domain analysis of guiding structures, by means of the proper choice of excitation and output parameter extraction.

2. Time-domain modelling of guiding structures.

To conduct time-domain calculations of an arbitrary guiding structure, we first divide its cross section into a grid of meshes. We then apply one of the three above mentioned algorithms to simulate the time evolution of fields over the grid.

2.1 VECTOR TWO-DIMENSIONAL FD-TD METHOD (2-DV FD-TD). — Under the assumption that waves propagate with the propagation constant β along the guide, and that the guide is parallel to the x-axis, the Maxwell's curl equations can be developed into the following form [2] :

$$\nabla \cdot \mathbf{J} = -C\,\partial V/\partial t \qquad \nabla V - \beta \mathbf{i}_x \times \mathbf{J}^h = -L\,\partial \mathbf{J}/\partial t$$
$$\nabla \cdot \mathbf{J}^h = -C^h\,\partial V^h/\partial t \qquad \nabla V^h - \beta \mathbf{i}_x \times \mathbf{J} = -L\,\partial \mathbf{J}^h/\partial t$$

where :

$$V = -E_x, \qquad V^h = -H_x, \quad \mathbf{J} = -\mathbf{i}_x \times \mathbf{H}_t, \quad \mathbf{J}^h = \mathbf{i}_x \times \mathbf{E}_t,$$
$$C = \varepsilon_x, \qquad C^h = \mu_x,$$
$$\mathbf{L} = \begin{bmatrix} \mu_y & 0 \\ 0 & \mu_z \end{bmatrix} \quad \mathbf{L}^h = \begin{bmatrix} \varepsilon_y & 0 \\ 0 & \varepsilon_z \end{bmatrix}. \tag{1}$$

Magnetic and electric potentials and currents V, V^h, $\mathbf{J}$, $\mathbf{J}^h$ have been introduced in [2] to facilitate easy approximation of curved boundaries of the guide's cross-section. As we show further in the paper, this notation additionally leads to the optimum modelling of excitation. Inhomogeneities and anisotropy of the medium filling the guide are accounted for directly, by means of putting appropriate values of C, C^h, $\mathbf{L}$, $\mathbf{L}^h$ for each individual mesh.

After discretizing the set of equations (1) with the use of central finite difference scheme as in [2], the equivalent network model of figure 1 is obtained. This model consists of two coupled LC-networks which support solutions of two 2-D scalar problems : one composed of longitudinal E and transversal H fields (V and $\mathbf{J}$ variables), and the other composed of longitudinal H and transversal E (V^h and $\mathbf{J}^h$ variables). The two LC-networks decouple at the cutoff frequency of the mode ($\beta = 0$).

2.2 COMPLEX TLM SCN ALGORITHM. — In figure 2 we present a fundamental structure of the symmetrical condensed node, as introduced by Johns [5]. It consists of six branches, each containing two transmission lines. In the TLM algorithm using the SCN pulses travel along the transmission lines with the velocity $v = a/\Delta t$, and are scattered at the nodes at time instants $k \cdot \Delta t$. The scattering is described by a scattering matrix $[S]$:

$$^{i}\mathbf{V} = [S]\,{}^{r}\mathbf{V} \tag{2}$$

where ${}^{r}\mathbf{V}$, ${}^{i}\mathbf{V}$ are column vectors each containing 12 pulses incident on/reflected onto the transmission lines at the node.

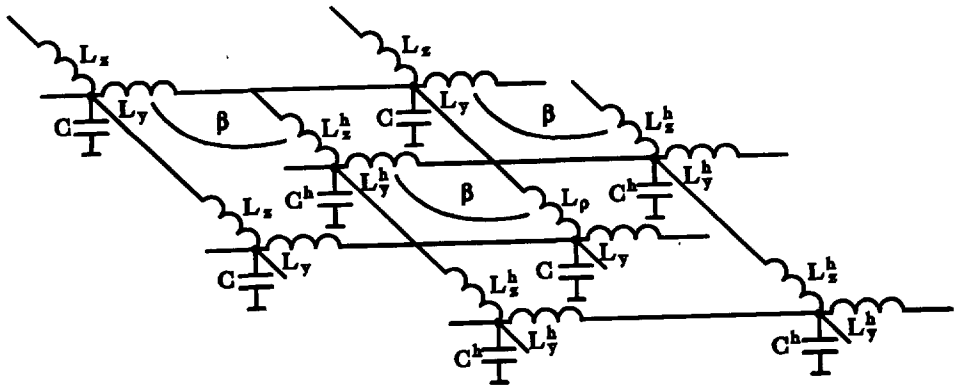

Fig. 1. — Equivalent network model of the 2-DV FD-TD algorithm.

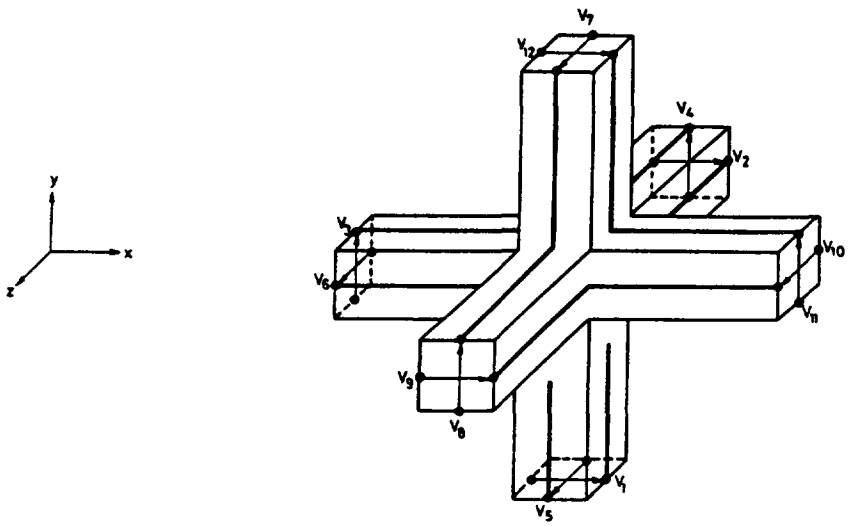

Fig. 2. — Symmetrical condensed 3-D TLM node.

In order to account for inhomogeneous and anisotropic media six additional stubs are introduced at the node. The 18×18 matrix $[S]$ can be found in [4].

In [3] Jin *et al.* proposed that for waves propagating with the propagation constant β along the guide the arms of the node which are parallel to the direction of propagation can be connected by a non-reciprocal phase shift :

$$
\begin{aligned}
{}^{i}V_{11}^{k+1} &= {}^{r}V_{3}^{k} \exp(j\beta a) \qquad {}^{i}V_{10}^{k+1} = {}^{r}V_{6}^{k} \exp(j\beta a) \\
{}^{i}V_{3}^{k+1} &= {}^{r}V_{11}^{k} \exp(-j\beta a) \quad {}^{i}V_{6}^{k+1} = {}^{r}V_{10}^{k} \exp(-j\beta a)
\end{aligned} \tag{3}
$$

where : *subscripts* 3, 6, 10, 11 correspond to the transmission lines of the node (Fig. 2) describing propagation along the considered guiding structure (x-axis), *superscripts* refer to time instants.

When compared with the 3-D SCN TLM, unchanged remain the nodal scattering matrix $[S]$ and the connections between nodes along the y and z-axis.

This approach permits to eliminate one space dimension from the analysis, in exchange however for introducing the complex numbers. In other words, instead of 12 (or 18) real variables per mesh required in the conventional SCN calculations we now need to store 24 (or 36) real variables per mesh. Consequently, the number of floating point operations per mesh per iteration also doubles.

2.3 2-DN SCN TLM ALGORITHM. — Let us propose a formally equivalent transformation of the symmetrical condensed node. Instead of pulses on lines 3, 6, 10, 11, we now consider their following linear combinations :

$$\underline{V}_3 = V_3 + V_{11} \quad \underline{V}_{11} = V_{11} - V_3 \quad \underline{V}_6 = V_6 + V_{10} \quad \underline{V}_{10} = V_{10} - V_6 \,. \tag{4}$$

The first observation is that the scattering at the node is now described by two separate matrix equations. Each of the matrices is composed of 6×6 (in inhomogeneous case 9×9) elements. In the homogeneous case the first equation involves only branches $\{B1\}$:

$$\{B1\} = \{1, 2, 9, 12, \underline{10}, \underline{11}\} \tag{5}$$

and the other-branches $\{B2\}$:

$$\{B2\} = \{4, 5, 7, 8, \underline{3}, \underline{6}\} \,. \tag{6}$$

Let us though examine how the transformation (4) modifies the form of the coupling equations (3). For example :

$$\begin{aligned} {}^{\mathrm{i}}\underline{V}_3^{k+1} = {}^{\mathrm{i}}V_3^{k+1} + {}^{\mathrm{i}}V_{11}^{k+1} &= {}^{\mathrm{r}}V_{11}^{k} \exp(-j\beta a) + {}^{\mathrm{r}}V_3^{k} \exp(j\beta a) = \\ &= [{}^{\mathrm{r}}V_3^{k} + {}^{\mathrm{r}}V_{11}^{k}] \cos(\beta a) + j[{}^{\mathrm{r}}V_3^{k} - {}^{\mathrm{r}}V_{11}^{k}] \sin(\beta a) \\ &= {}^{\mathrm{r}}\underline{V}_3^{k} \cos(\beta a) - j\, {}^{\mathrm{r}}V_{11}^{k} \sin(\beta a) \,. \end{aligned} \tag{7}$$

To be able to satisfy equations (3), Jin *et al.* had to admit complex values of pulses on all branches :

$$V_\ell = U_\ell + jW_\ell \quad \text{for} \quad \ell = 1, 2, \ldots, 18 \,. \tag{8}$$

On the contrary, the coupling equations of the form (7) can be satisfied with all pulses on branches $\{B1\}$ having purely real values :

$$V_\ell = U_\ell \quad \text{for} \quad \ell \in \{B1\} \tag{9}$$

and all pulses on branches $\{B2\}$ purely imaginary :

$$V_\ell = jW_\ell \quad \text{for} \quad \ell \in \{B2\} \,. \tag{10}$$

We then obtain the coupling equations :

$$\begin{aligned} {}^{\mathrm{i}}\underline{W}_3^{k+1} &= {}^{\mathrm{r}}\underline{W}_3^{k} \cos(\beta a) + {}^{\mathrm{r}}\underline{U}_{11}^{k} \sin(\beta a) \\ {}^{\mathrm{i}}\underline{U}_{11}^{k+1} &= -{}^{\mathrm{r}}\underline{U}_{11}^{k} \cos(\beta a) + {}^{\mathrm{r}}\underline{W}_3^{k} \sin(\beta a) \\ {}^{\mathrm{i}}\underline{W}_6^{k+1} &= {}^{\mathrm{r}}\underline{W}_6^{k} \cos(\beta a) + {}^{\mathrm{r}}\underline{U}_{10}^{k} \sin(\beta a) \\ {}^{\mathrm{i}}\underline{U}_{10}^{k+1} &= -{}^{\mathrm{r}}\underline{U}_{10}^{k} \cos(\beta a) + {}^{\mathrm{r}}\underline{W}_6^{k} \sin(\beta a) \,. \end{aligned} \tag{11}$$

The nodal scattering matrices for the homogeneous case are presented in table I. Since these matrices are also real, we have reduced the complex problem to real number calculations, with half of the memory cells and half of the operations needed for [3] (cf. Tab. II).

Table I. — *Coupling matrices of the new transformed two-dimensional* TLM *node in homogeneous medium.*

$$\begin{bmatrix} {}^{r}U_1 \\ {}^{r}U_2 \\ {}^{r}U_9 \\ {}^{r}U_{12} \\ {}^{r}U_{10} \\ {}^{r}U_{11} \end{bmatrix} = \frac{1}{2} \begin{bmatrix} 0 & 1 & 1 & 0 & 0 & -1 \\ 1 & 0 & 0 & 1 & -1 & 0 \\ 1 & 0 & 0 & 1 & 1 & 0 \\ 0 & 1 & 1 & 0 & 0 & 1 \\ 0 & -2 & 2 & 0 & 0 & 0 \\ -2 & 0 & 0 & 2 & 0 & 0 \end{bmatrix} \cdot \begin{bmatrix} {}^{i}U_1 \\ {}^{i}U_2 \\ {}^{i}U_9 \\ {}^{i}U_{12} \\ {}^{i}U_{10} \\ {}^{i}U_{11} \end{bmatrix}$$

$$\begin{bmatrix} {}^{r}W_4 \\ {}^{r}W_5 \\ {}^{r}W_7 \\ {}^{r}W_8 \\ {}^{r}W_3 \\ {}^{r}W_6 \end{bmatrix} = \frac{1}{2} \begin{bmatrix} 0 & 1 & -1 & 0 & 0 & 1 \\ 1 & 0 & 0 & -1 & 1 & 0 \\ -1 & 0 & 0 & 1 & 1 & 0 \\ 0 & -1 & 1 & 0 & 0 & 1 \\ 0 & 2 & 2 & 0 & 0 & 0 \\ 2 & 0 & 0 & 2 & 0 & 0 \end{bmatrix} \cdot \begin{bmatrix} {}^{i}W_4 \\ {}^{i}W_5 \\ {}^{i}W_7 \\ {}^{i}W_8 \\ {}^{i}W_3 \\ {}^{i}W_6 \end{bmatrix}$$

Table II. — *Comparison of numerical effectiveness of the three time-domain algorithms. Separately considered are basic meshes (i.e., filled with one isotropic medium which we assume to be a « reference » medium for the circuit) and meshes filled with any other type of medium.*

	2-DV FD-TD*		Complex SCN TLM		2-DV SCN TLM	
	No. var.	No. op.	No. var.	No. op.	No. var.	No. op.
basic mesh $\varepsilon_r = 1$ $\mu_r = 1$	6	(+) 20 (: 2) 2 (×) 4	24	(+) 80 (: 2) 12 (×) 16	12	(+) 24 (: 2) 8 (×) 8
other mesh $\varepsilon_r > 1$ $\mu_r > 1$	6	(+) 20 (×) 10	36	(+) 140 (: 4) 24 (×) 28	18	(+) 62 (: 4) 12 (×) 14

No. var. — number of memory locations per mesh to store real variables.

No. op. — number of floating point operations executed per mesh per iteration ; we distinguish additions (+), multiplications (×) and divisions by powers of 2.

(*) Stability properties of the three methods are such that with equal mesh size, the time step in the 2-DV FD-TD can be greater by a factor of $\sqrt{2}$ than the time step in both the Complex SCN TLM and the 2-DV SCN TLM. Therefore if we consider the total number of computer operations needed to simulate a desired period of time, relative efficiency of the 2-DV FD-TD is still by 30 % better than it directly follows from table II.

In figure 3 we show the structure of the modified symmetrical condensed node. Analogously to the above discussed FD-TD algorithm, this node is composed of two nodes representing the solutions of two 2-D scalar problems (longitudinal E + transversal H ; longitudinal H + transversal E). A link between the two sub-nodes provides the coupling of the two scalar solutions above the cutoff frequency.

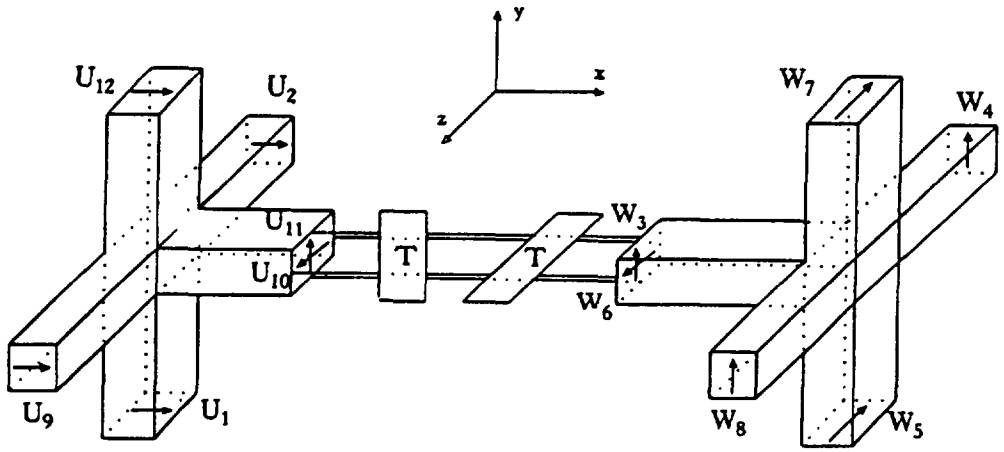

Fig. 3. — New transformed symmetrical condensed node for 2-DV calculations.

3. Exciting the time-domain models.

Essentially, the three methods presented in section 2 reduce a 3-D problem of analyzing dispersion characteristics of a guiding structure — to a vector 2-D eigenvalue problem, that is to calculating eigenfrequencies and then eigenmodes of a planar resonator. We now have to initiate the process of wave propagation in the resonator. Ideally, the modelled excitation should resemble the distribution of fields of the analyzed eigenmodes. Although some work has been started along the line of using modal templates [6, 7], the single point excitation is generally preferred for its simplicity and versatility. In either case, the classically used excitation procedure [7, 9, 10] consists in directly setting the initial value of the selected electromagnetic field components at selected points, for example of the field component A situated at the input $(x1, y1, z1)$:

$$A(x1, y1, z1) = 1 \quad \text{at} \quad t = 0 \tag{12}$$

with all other field components equal zero. To extract the eigenfrequencies of the resonator, the Fourier transform of the field component $B(x2, y2, z2)$ is plotted at the output point $(x2, y2, z2)$. The maxima of the Fourier transform $B(x2, y2, z2, \omega)$ indicate the eigenfrequencies. This classical approach still exhibits several disadvantages which will be demonstrated in comparison with the new approach introduced herein.

Let us consider the finite-difference form of an equation for updating the longitudinal E-field. Using the circuit notation as in equations (1), we can write :

$$U(t + \Delta t/2) = U(t - \Delta t/2) - [I_1(t) + I_2(t) - I_3(t) - I_4(t)]\, \Delta t/C \ . \tag{13}$$

The meaning of the symbols is explained in figure 4a. Let us now add an excitation branch denoted by number 5 (Fig. 4b). The current in the branch 5 is obtained from :

$$I(t) = I(t - \Delta t) - [U_0(t - \Delta t/2) - U(t - \Delta t/2) - RI(t - \Delta t)]\, \Delta t/L' \qquad (14)$$

and the voltage equation (13) modifies to :

$$U(t + \Delta t/2) = U(t - \Delta t/2) - [I_1(t) + I_2(t) - I_3(t) - I_4(t) + I_5(t)]\, \Delta t/C\ . \qquad (15)$$

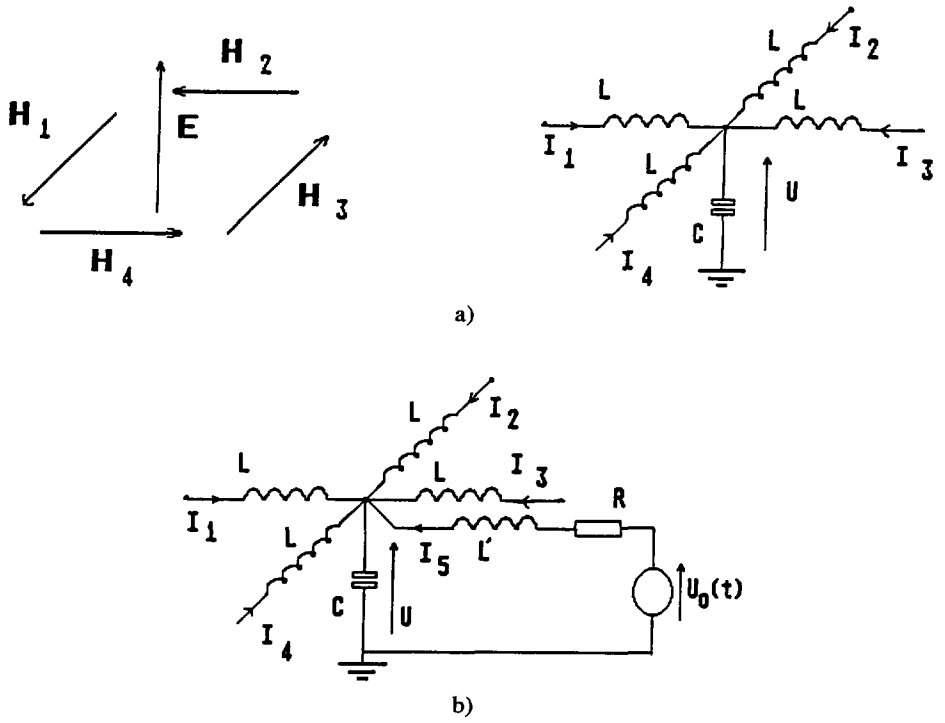

Fig. 4. — a) Fields considered in one of the Maxwell's equations and the equivalent scheme of the finite-difference approximation. b) The same scheme supplemented by the excitation branch.

To extract the output information, we consider the Fourier transform of I_5 which has minima for eigenfrequencies of the structure. It must be noted that at a resonant frequency in the steady state the input impedance of the circuit seen from the branch 5 tends to infinity, and so the resistance R does not influence the value of the resonant frequency. For frequencies different from the resonance however, energy is dissipated in R.

We have applied the new form of excitation to various 2-D and vector 2-D eigenvalue problems. We have observed the following advantages over the classical approach :

1. the Fourier transform of the output signal exhibits almost no ripples and its minima are clearly visible (contrast Fig. 5 to Fig. 6) ;

2. the proper values of resonant frequencies are usually obtained with a smaller number of iterations ;

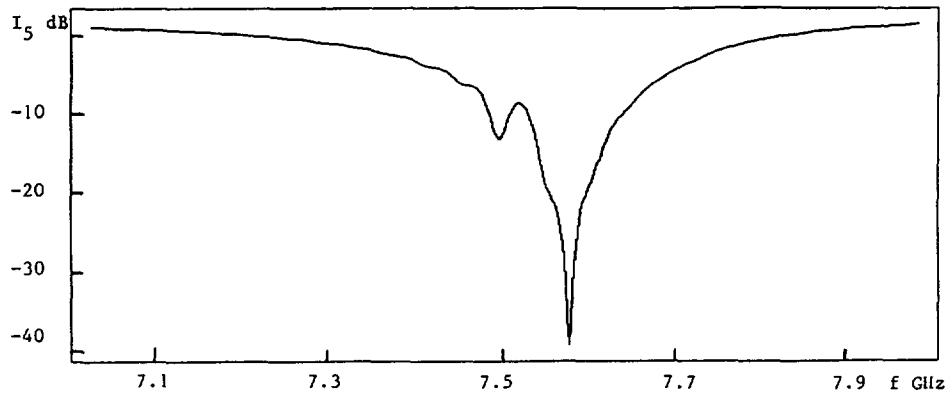

Fig. 5. — The output signal in the new excitation scheme for a resonator with two eigenfrequencies, at 7.57 GHz (strongly coupled to the input) and 7.49 GHz (weakly coupled to the input) after 15 000 iterations.

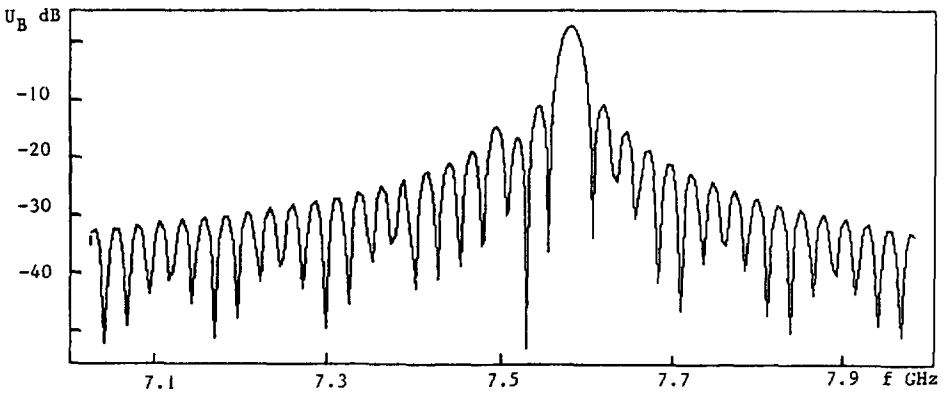

Fig. 6. — The output signal after 25 000 iterations for the same resonator as in figure 5 but applying the classical excitation.

3. the new type of excitation permits to distinguish even resonances very close to each other and excited with different coupling factors. In figure 5, we present the results of calculations for a circuit with two resonances separated in frequency by 1 %, and one of them being weakly coupled to the input. After 15 000 iterations our method enables us to clearly distinguish the two resonances and to point them out with the frequency error less than 0.1 %. Figure 6 shows the results of the analysis of the same problem after 25 000 iterations, but with the use of the classical excitation. In this case it seems difficult enough to distinguish the strong resonance from numerical ripples, while the weak resonance is practically undetectable.

Apart from determining the eigenfrequencies, the time-domain algorithms can produce the field distribution of any particular eigenmode. To achieve this, we excite the resonator by a sinusoidal signal of the previously calculated resonant frequency. In view of this application the new form of excitation also proves advantageous since other modes (generated by the transitional period) are relatively quickly damped by the source resistance R. The unperturbed image of the desired field distribution is obtained, as that in figure 7 showing the dominant mode in a rectangular waveguide. On the contrary, as result of using the classical excitation even after a long computation time the dominant mode is mixed with the higher ones (Fig. 8).

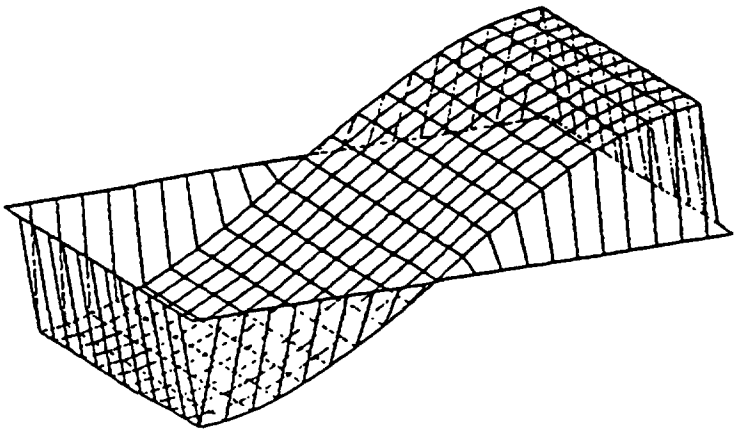

Fig. 7. — Dominant mode in a rectangular waveguide obtained after 1 500 iterations — the new type of excitation applied in a corner.

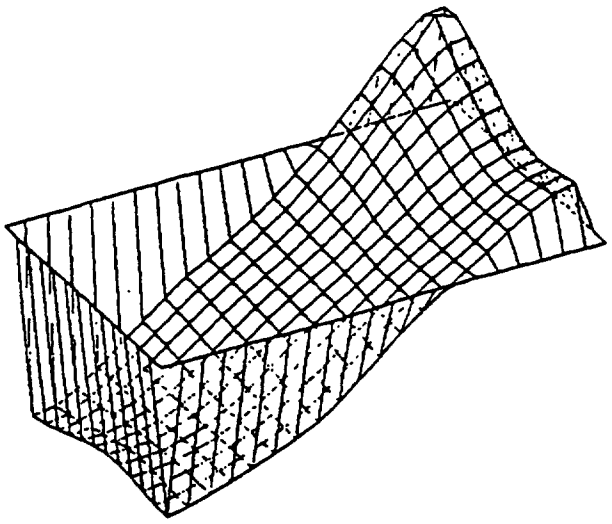

Fig. 8. — The same mode and the same waveguide as in figure 7, but after 15 000 iterations — the classical excitation applied.

4. Example of analysis and conclusions.

To demonstrate the validity of the vector 2-D approach to the analysis of dispersive guiding structures, we first compare the results of this approach with the direct 3-D one. We consider the case of a finline after [7]. In figure 9 we present the dispersion characteristics of this line as obtained with the 2-DV SCN algorithm introduced in this work (crosses), with the 3-D FD-TD [7] (points) and with the spectral domain method [7] (continuous line). Clearly, the agreement is very good.

We have run several examples to verify if the Complex SCN TLM and the 2-DV SCN TLM give the same results. It has been confirmed that the results obtained by the Complex SCN TLM and the 2-DV SCN TLM are indistinguishable and thus out of these two methods the 2-DV SCN TLM as more effective is recommended.

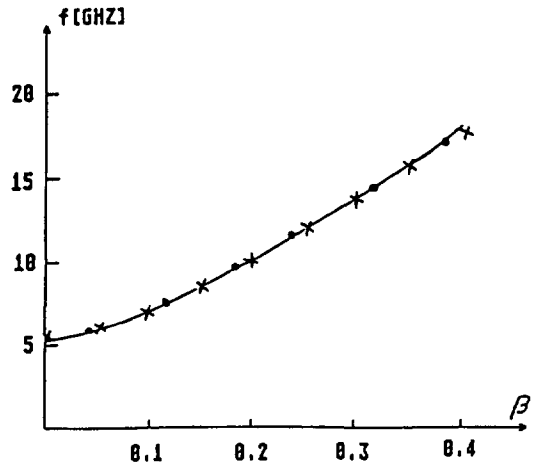

Fig. 9. — Dispersion characteristics of a finline-results by the 2-DV SCN algorithm (crosses), the 3-D FD-TD (points) and the spectral method [7] (continuous line).

We have compared several examples which had been described before in the literature with calculations by the 2-DV SCN TLM and 2-DV FD-TD. Typical result is presented in figure 10 where both methods are in a very good agreement with the available reference. There are however some small differences between them :

— The 2-DV SCN TLM method gives smaller numerical dispersion. To obtain similar level of dispersion in the 2-DV FD-TD method we have to decrease the mesh size by about 30 %.

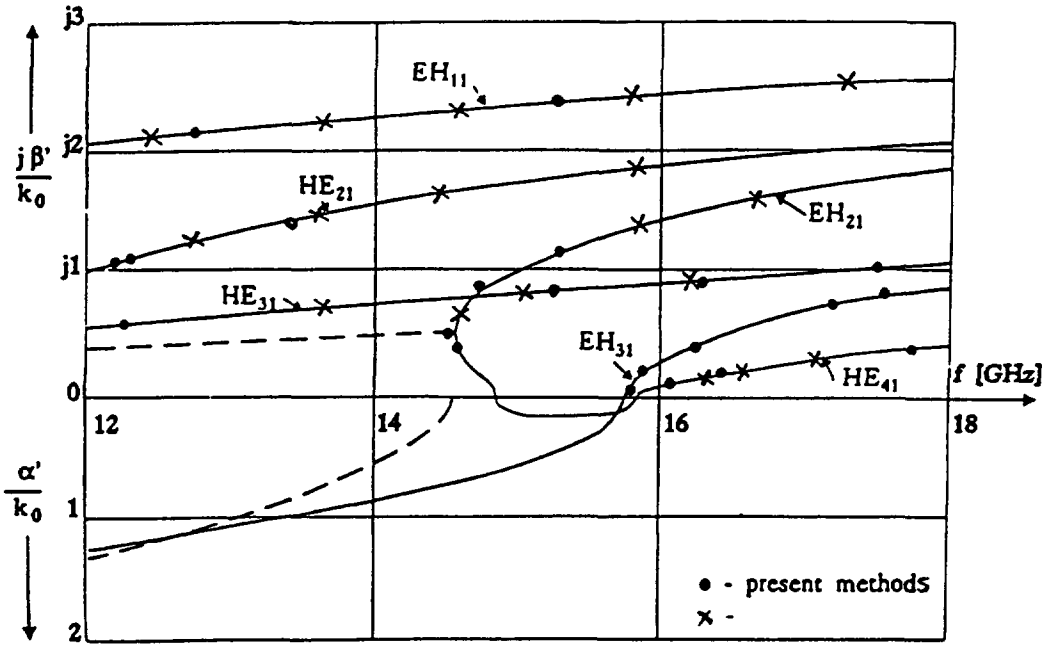

Fig. 10. — Dispersion characteristics of a shielded image guide after [6] (continuous line) with the results of calculations using the 2-DV FD-TD algorithm (points) and the 2-DV SCN TLM algorithm (crosses).

— The 2-DV FD-TD method requires much less computer operations per mesh and per iteration and thuis is more effective even when we take into account some mesh reduction needed to compensate bigger dispersion. Computer resources needed for all three methods are compared in table II.

— The 2-DV FD-TD method can directly use so called « modified meshes » [11] introduced to account for curved boundaries. This further improves its effectiveness for arbitrary shapes. Corresponding procedure for the 2-DV SCN TLM has not been reported yet and seems to be difficult to introduce.

We have tried to employ the described algorithms to lossy and open (leaky) structures, this however requires some additional remarks. It is not possible to directly incorporate complex values of a propagation constant. At first it may seem that the complex notation of the algorithm [4] allows for such a direct approach — but in fact also in this case the complex wave numbers cannot be admitted since they would cause instability of calculations. Therefore in all three discussed methods losses are considered indirectly, by means of a quality factor of a resonator [4]. We have applied this approach also to the 2-DV SCN TLM and 2-DV FD-TD algorithms and confirmed that it is fairly accurate for small losses.

References

[1] YEE K. S., Numerical solution of initial boundary value problems involving Maxwell's equations in isotropic media, *IEEE Trans. Antennas Propag.* **AP-14** (1966) 302-307.

[2] MROCZKOWSKI C., GWAREK W., Microwave circuits described by two-dimensional vector wave equation and their analysis by FD-TD method, XXI European Microwave Conference (Stuttgart 1991) 866-871.

[3] JIN H., VAHLDIECK R., XIAO S., An improved TLM full-wave analysis using a two-dimensional mesh, *IEEE MTT Symp. Digest* (Boston 1991) 675-678.

[4] JIN H., VAHLDIECK R., XIAO S., A full-wave analysis of arbitrary guiding structures using a two-dimensional TLM mesh, XXI European Microwave Conference (Stuttgart 1991) 205-210.

[5] JOHNS P. B., A Symmetrical Condensed Node for the TLM Method, *IEEE Trans. Microwave Theory Tech.* **MTT-35** (1987) 370-377.

[6] STRUBE S., ARNDT E., Rigorous hybrid mode analysis of the transition from waveguide to shielded dielectric image line, *IEEE Trans. Microwave Theory Tech.* **MTT-33** (1987) 391-401.

[7] CHOI D. H., HOEFER W. J. R., The Finite-Difference Time-Domain Method and its Application to Eigenvalue Problems, *IEEE Trans. Microwave Theory Tech.* **MTT-34** (1986) 1464-1470.

[8] GWAREK W., Analysis of arbitrarily-shaped two-dimensional microwave circuits by finite-difference time-domain method, *IEEE Trans. Microwave Theory Tech.* **MTT-36** (1988) 738-744.

[9] ITOH T., Numerical Techniques for Microwave and Millimeter Wave Passive Structures (New York, Johns Wiley & Sons, Inc., 1989).

[10] FURSE C. M., MATHUR S. P., GANDHI O. P., Improvements to the Finite-Difference Time-Domain Method for Calculating the Radar Cross Section of a Perfectly Conducting Target, *IEEE Trans. Microwave Theory Tech.* **MTT-38** (1990) 919-927.

[11] GWAREK W., Analysis of arbitrary-shaped planar ircuit — a time-domain approach, *IEEE Trans. Microwave Theory Tech.* **MTT-33** (1985) 1067-1071.